IBRACON Structures and Materials Journal
Revista IBRACON de Estruturas e Materiais
ISSN 1983-4195 *ismj.org*

ORIGINAL ARTICLE

Nonlinear analysis of monolithic beam-column connections for reinforced concrete frames

Análise não linear de ligações viga-pilar monolíticas em pórticos de concreto armado

Gerson Alva[a]
Alexandre Tsutake[a]

[a]Universidade Federal de Uberlândia – UFU, Faculdade de Engenharia Civil, Uberlândia, MG, Brasil

Received 10 March 2019
Accepted 12 February 2020

Abstract: This paper deals with nonlinear analysis of deformability of monolithic beam-column connections for bending moments in framed reinforced concrete structures. Due to the simplicity, the connections deformability is considered by using an analytical model of moment-rotation curve. Material nonlinearity of the structural elements is considered by using the flexural stiffness obtained in moment-curvature relationship of the sections. The formulation of the analytical model to obtain the relative rotations between beam and column and the formulation to construct moment-curvature curves is deduced and presented to allow the computational implementation in structural analysis software. The numerical simulations carried out in this study indicated that even in the case of monolithic connections, taking into account the bending moment deformability of the connections leads to significantly better results than the hypothesis of fully rigid connections.

Keywords: bending deformability, beam-column connections, nonlinear analysis, reinforced concrete structures, structural analysis.

Resumo: Este trabalho trata da análise não linear da deformabilidade de ligações monolíticas viga-pilar de concreto armado devido ao momento fletor em estruturas reticuladas de concreto armado. Em função da simplicidade, a deformabilidade das ligações é considerada por meio de modelo analítico de curva momento-rotação e a não-linearidade física dos elementos estruturais, por meio da rigidez à flexão obtida em relações momento-curvatura das seções. A formulação do modelo analítico para a obtenção das rotações relativas entre viga e pilar e a formulação relacionada com a geração das curvas momento-curvatura foram deduzidas e apresentadas, com o intuito de permitir a implementação desses modelos em rotinas computacionais. As simulações numéricas realizadas neste trabalho comprovaram que, mesmo em se tratando de ligações monolíticas, levar em conta a deformabilidade das ligações ao momento fletor conduz a resultados significativamente melhores que a hipótese de ligações perfeitamente rígidas.

Palavras-chave: deformabilidade ao momento fletor, ligações viga-pilar, análise não linear, estruturas de concreto armado, análise estrutural.

How to cite: G. Alva and A. Tsutake, "Nonlinear analysis of monolithic beam-column connections for reinforced concrete frames," *Rev. IBRACON Estrut. Mater.*, vol. 13, no. 5, e13515, 2020, https://doi.org/10.1590/S1983-41952020000500015

1 INTRODUCTION

In reinforced concrete structures, cracking of concrete, plastification of materials and bond-slip behavior between steel and concrete are responsible for the material nonlinear behavior of these structures.

For Ultimate Limit State procedures in the design of frames structures for buildings, the material nonlinearity of structural elements in global analysis can be considered simply by flexural stiffness reductions of these elements for use in linear analysis, as recommended by NBR 6118 [1] and others international codes. Alternatively, in the need for

Corresponding author: Gerson Alva. E-mail: alva_gerson@yahoo.com.br
Financial support: CNPq (Process: 308720/2018-0), CAPES (Process: 1769743).
Conflict of interest: Nothing to declare.

checking the design based on simplified linear analysis, nonlinear analysis can be employed with the use of moment-curvature relationships of the sections. In this case, the framed structure is discretized, and the flexural stiffness of each section is calculated as a function of its moment-curvature relationship.

The nonlinear effects that occur in beam-column connections of monolithic reinforced concrete structures - such as the slippage of flexural reinforcement of the beams in the joint region and the formation of flexural cracks at the beam extremity - induce the generation of relative rotations between the beam and the column. Thus, monolithic connections, strictly speaking, are not perfectly rigid under bending moment. Evidently, there is greater concern with the bending deformability in precast concrete structures. However, the consideration of bending deformability in monolithic connections brings benefits to the structural analysis justified by the greater precision in obtaining stresses and displacements - as shown in this paper.

Due to the simplicity and the good results they can provide, analytical models are the most attractive way in design procedures to consider the effects of the slippage of the beam reinforcement inside the column and the effects induced by the flexural cracks at the beam extremity on the bending deformability. Examples of these models can be found in Paultre et al. [2], Sezen and Moehle [3], Sezen and Setzler [4], Kwak and Kim [5], Ferreira et al. [6], Alva et al. [7] and Alva and El Debs [8], the latter being emphasized in this study.

The Alva and El Debs [8] model was proposed for exterior beam-column connections. Due to the formatting of the formulation, this model can be easily implemented in software programs for nonlinear analysis of frames that use moment-curvature relationships for the consideration of the material nonlinearity of structural elements.

There are three central objectives of this paper, namely:

- Complement the investigations on the efficiency of the model proposed by Alva and El Debs [8] to consider the bending deformability caused by the slippage of flexural reinforcement of the beams in the joint region;
- Present an analytical formulation to obtain moment-curvature relationships of reinforced concrete rectangular sections, aiming to consider the material nonlinearity of beams and columns and the application of the analytical model proposed by Alva and El Debs [8] in nonlinear analysis of reinforced concrete frames;
- Show the efficiency of the constitutive models employed for considering material nonlinearity of the structural elements (by moment-curvature relationships) and bending deformability in nonlinear analysis of framed reinforced concrete structures.

2 PREVIOUS STUDIES

Although there are numerous researches in the literature (especially international) on the behavior of monolithic beam-column connections, few studies that focus on analytical models for considering the deformability of connections subjected to bending moment are found.

There are analytical models that exclusively consider the portion of rotation resulting from the slippage of the flexural reinforcement in the anchorage region, such as those found in Paultre et al. [2], Sezen and Moehle [3] and Sezen and Setzler [4]. Paultre et al. [2] used a tri-linear moment-rotation curve with points defined by the cracking of the concrete, yielding of the reinforcement and failure of the beam section. For the calculation of the rotations, the authors used a simplified distribution of bond stresses in the elastic and inelastic ranges (after reinforcement yielding). Sezen and Moehle [3] and Sezen and Setzler [4] proposed an analytical model applicable to the case of slippage of longitudinal tension reinforcement of columns (anchored in foundations) or beams (anchored in beam-column joints). As in Paultre et al. [2], Sezen and Moehle [3] and Sezen and Setzler [4] used a simplified distribution of bond stresses but proposed an additional simplification regarding the distribution of the axial strains of the reinforcement in the anchorage regions.

Among the analytical models that consider both portions of relative rotations - those resulting from slippage of the flexural reinforcement inside the joint and those resulting from cracking at the beam extremity - the following models can be cited: Kwak and Kim [5], Ferreira et al. [6], Alva et al. [7] and Alva and El Debs [8]. Kwak and Kim [5] proposed an analytical model which accounts for the effects of relative rotations by reducing the flexural stiffness along the equivalent plastic length of the beams (extremities). The total rotation calculated by the model is associated with the slippage of flexural reinforcement of the beam inside the column added the rotation induced by the crack at the beam-column interface. These rotations are obtained by solving the differential equations which represent the bond-slip behavior. The analytical models presented in Ferreira et al. [6], Alva et al. [7] and Alva and El Debs [8] take into account the two rotation portions, but consider that the slippage induced by flexural cracking occurs in a certain length of the beam extremity, associated with its effective depth. Ferreira, El Debs and Elliott [6] model was proposed for

connections between precast elements, being later extended to monolithic connections, as presented in Alva et al. [7]. Subsequently, Alva and El Debs [8] presented a specific analytical model for exterior beam-column monolithic connections. This model has the advantage of including in the formulation parameters not considered in Alva et al. [7], such as bond strength in the joint region and the diameter of the beam reinforcement bars, a parameter that influences the flexural crack widths in this member (beam).

3 MODEL PROPOSED BY ALVA AND EL DEBS [8]

Based on the conceptual model proposed by Ferreira et al. [6], Alva and El Debs [8] proposed a theoretical model which is capable of representing the bond-slip behavior of the reinforcement without the need for parameters from experimental tests. In addition, it can be easily implemented in software programs for structural analysis. In this model, it is assumed that the bending deformability is the result of two mechanisms, which produce relative rotations between the beam and the column (Figure 1):

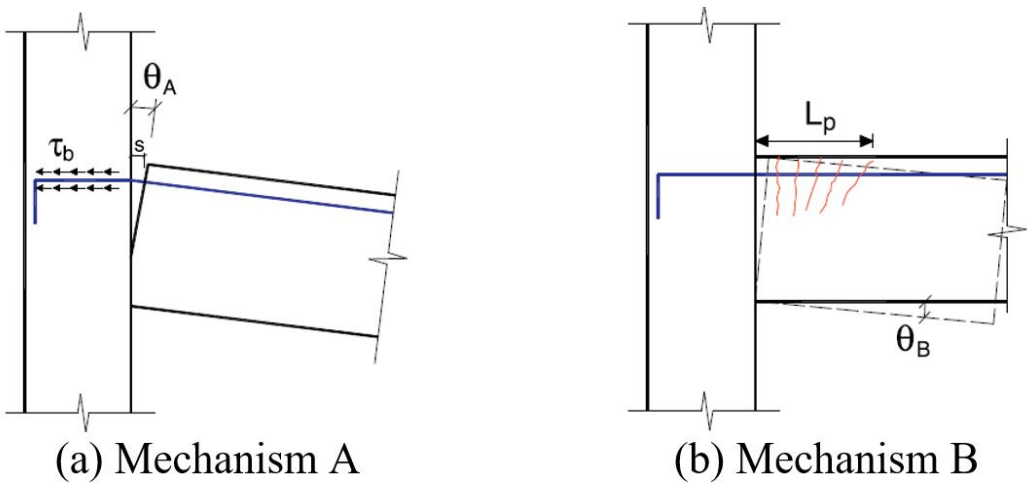

Figure 1. Deformation mechanisms: Alva and El Debs model [8]

- Mechanism A: Relative rotations produced by the slippage of tensile reinforcement of the beam inside the column (joint region);
- Mechanism B: Relative rotations produced by the cumulative effect of the slippage caused by flexural cracks formed along the plastic hinge length L_p (region where there is a greater concentration of cracks)

The total beam-column rotation related to the bending deformability consists of the sum of the rotations caused by the two mechanisms (Equation 1):

$$\theta = \theta_A + \theta_B \tag{1}$$

where θ_A is the rotation due to Mechanism A and θ_B is the rotation due to Mechanism B.

3.1 Mechanism A

The contribution of Mechanism A is calculated through the model proposed by Sezen and Moehle [3], which assumes the distribution of bond and axial stresses of the steel bar as shown in Figure 2. Bond stresses are divided into two uniformly distributed portions: τ_{by} for the elastic range ($\varepsilon_s \leq \varepsilon_y$) and τ_{bu} for the inelastic range ($\varepsilon_s > \varepsilon_y$).

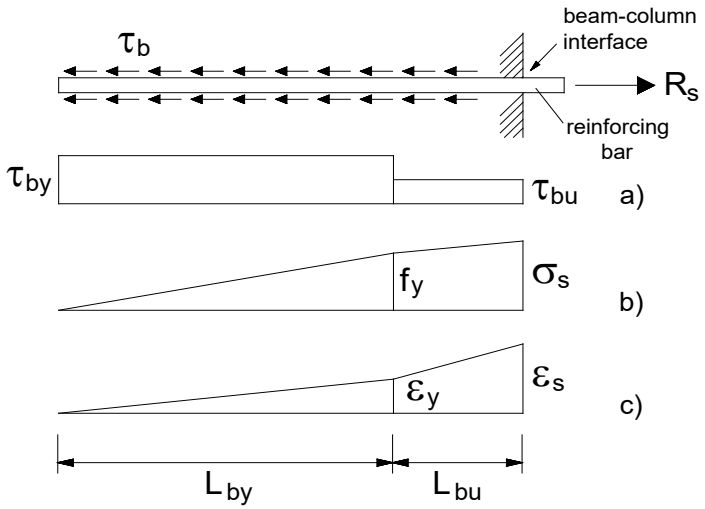

Figure 2. Bond-slip model proposed by Sezen and Moehle [3]: (a) bond stress distribution; (b) axial stress distribution; (c) axial strain distribution.

The values proposed by the authors are $\tau_{by} = 1{,}0\sqrt{f_c}$ and $\tau_{bu} = 0{,}5\sqrt{f_c}$, where f_c is the concrete compressive strength in MPa. Thus, the slip (s) of the steel bar is obtained from the difference between the steel bar strain (ε_s) and the concrete strain (ε_c):

$$s = \int_0^x (\varepsilon_s - \varepsilon_c)\, dx \tag{2}$$

Disregarding the concrete strain (very small when compared with steel bar), solving the Equation 2 and applying the equilibrium equations, Sezen and Moehle [3] deduced Equations 3 and 4 for calculating the slip.

Elastic range ($\varepsilon_s \leq \varepsilon_y$):

$$s = \frac{\varepsilon_s \cdot \sigma_s \cdot \varnothing}{8 \cdot \tau_{by}} \tag{3}$$

Inelastic range ($\varepsilon_s > \varepsilon_y$):

$$s = \frac{\varepsilon_y \cdot f_y \cdot \varnothing}{8 \cdot \tau_{by}} + \frac{(\varepsilon_y + \varepsilon_s) \cdot \varnothing \cdot (\sigma_s - f_y)}{8 \cdot \tau_{bu}} \tag{4}$$

where

ε_s is the steel bar axial strain;

σ_s is the steel bar axial stress;

$\varnothing$ is the steel bar diameter;

ε_y is the steel strain at yield strength;

f_y is the steel yield strength of steel.

Knowing the slip resulting from Mechanism A, it is possible to calculate the respective relative rotation between the beam and column elements:

$$\theta_A = \frac{s}{d - x} \tag{5}$$

where d is the effective depth of the beam and x is the neutral axis depth of the beam.

As a simplification, Alva and El Debs [8] suggest that constant values of neutral axis depth x be used in each range. In the elastic range, the authors suggest the value $x = x_{II}$ corresponding to Stage II (cracked section), since this value becomes practically constant after crack stabilization. In the inelastic range, the authors suggest the value $x = x_u$ corresponding to the ultimate moment, since in Stage III there is a rapid stabilization of the x values between the yielding moment and the ultimate moment.

3.2 Mechanism B

The relative rotation related to Mechanism B is caused by the sum of the slips induced by the flexural cracks at the extremity of the beam next to the column along the length L_p. As shown in Figure 3, cracks are supposed equally spaced (s_R) in Alva and El Debs [8] model. The corresponding slips s_i are assumed equal to half the value of the crack width w_i .

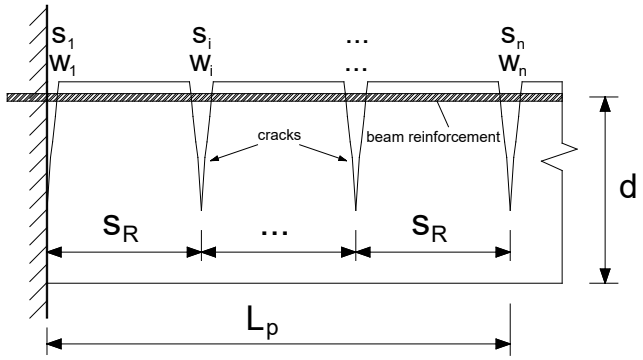

Figure 3. Mechanism B: slips caused by flexural cracks - Alva and El Debs model [8]

Therefore, the total rotation along the length L_p induced by a number of cracks n is given by Equation 6.

$$\theta_B = \sum_{i=1}^{n} \frac{s_i}{d - x_i} = \sum_{i=1}^{n} \frac{0,5 \cdot w_i}{d - x_i} \tag{6}$$

where

x_i is the neutral axis depth at the section where the crack occurs (crack width: w_i). In this case, the simplification suggested by the authors can be used ($x_i = x_{II}$ or $x_i = x_u$).

Assuming small differences between the values of w_i along the length L_p, it is possible to obtain a single crack opening value in that length by the Equation 7:

$$w = s_R \cdot (\varepsilon_{sm} - \varepsilon_{cm}) \tag{7}$$

where

s_r is the crack spacing;

$\varepsilon_{sm} - \varepsilon_{cm}$ is the difference between the average reinforcement strain and the average concrete strain.

Again ignoring the strain of the concrete in tension and knowing that the spacing between cracks s_r allows the evaluation of the probable number of cracks along the length L_p, Alva and El Debs [8] deduced the following expression for relative rotation resulting from Mechanism B:

$$\theta_B = 0,5 \cdot \left(L_p + s_R\right) \cdot \left(\frac{\varepsilon_{sm}}{d-x}\right) = 0,5 \cdot \left(L_p + s_R\right) \cdot \frac{1}{r} \tag{8}$$

where
x is the neutral axis depth, which can be simplified as suggestion of the authors ($x = x_{II}$ or $x = x_u$);
ε_{sm} is the average deformation in the reinforcement, considering the contribution of tensioned concrete (tension stiffening);
$1/r$ is the curvature of the beam section, considering the contribution of tensioned concrete (tension stiffening).

Knowing the bending moment M at the end of the beam, it is possible to find the axial stresses and strains in the reinforcement (Equations 3 and 4) and also the curvature $1/r$ of Equation 8. Hence, the model proposed by Alva and El Debs [8] can be deduced, according to Equations 9 and 10.

In the elastic range: $M \leq M_y$

$$\theta = C_1 \cdot M^2 + C_2 \cdot \left(\frac{1}{r}\right) \tag{9}$$

In the inelastic range: $M_y < M \leq M_u$

$$\theta = C_1 \cdot M_y^{\,2} + C_2 \cdot \left(\frac{1}{r}\right) \tag{10}$$

where
M_y is the beam yielding moment;
M_u is the beam ultimate moment;
C_1 is the constant related to Mechanism A, given by Equation 11.

$$C_1 = \frac{\varnothing}{8 \cdot E_s \cdot \tau_{by} \cdot \left(d-x\right) \cdot A_s^{\,2} z^2} \tag{11}$$

E_s is the steel modulus of elasticity;
A_s is the beam area of flexural reinforcement;
z is the lever arm between the tensile and compressive forces in the beam section;
C_2 is the constant related to Mechanism B, given by Equation 12.

$$C_2 = 0,5 \cdot \left(L_p + s_R\right) \tag{12}$$

The spacing between cracks s_R can be evaluated from codes expressions or from formulations found in literature. In this paper, the expression presented in Eurocode 2 [9] was used:

$$s_R = k_3.c + \frac{k_1.k_2.k_4.\varnothing}{\rho_{eff}} \tag{13}$$

where
$\varnothing$ is the diameter of the beam steel reinforcement bars;
k_1 is a coefficient which considers for the bond properties of the reinforcement steel bars (equal to 0.8 for high-bond bars and equal to 1.6 for plain surface bars);
$k_2 = 0{,}5$; $k_3 = 3{,}4$; $k_4 = 0{,}425$;
c is the concrete cover;
$\rho_{eff} = \frac{A_s}{A_{c,eff}}$
$A_{c,eff}$ is the effective tension area of concrete protected by the steel reinforcement bars along the height $h_{c,eff}$, which assumes the lowest value between $2{,}5(h-d)$, $(h-x)/3$ or $h/2$ (see Figure 4).

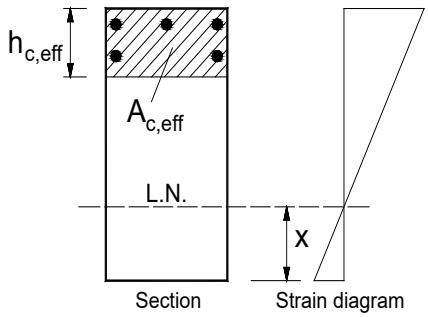

Figure 4. Definition of effective area $A_{c,eff}$ - Eurocode 2 [9]

4 MOMENT-CURVATURE RELATIONS

This item presents the analytical formulation for obtaining the moment-curvature relationships necessary to consider the material nonlinearity of the structural members (beam and column). It should be noted that the model proposed by Alva and El Debs [8] uses the curvature value at the beam end (next to the joint region) to calculate the relative rotation component resulting from flexural cracks (Mechanism B). Item 4.1 presents the analytical formulation for the construction of moment-curvature curves of rectangular sections from the integration of the material stresses and the equilibrium and strain compatibility equations, applicable for concrete up to C50. For concretes between C55 and C90, the analytical formulation can be found in Alva [10]. The analytical formulation of item 4.1 was implemented in a computational procedure in FORTRAN language and the results were validated by free and commercial software for structural analysis found in Brazil, as presented in Alva [10]. The computational procedure was used in the examples presented in item 5.

4.1 Integration of stresses and equilibrium equations in reinforced concrete section (columns and beams)

To understand the problem of rectangular sections subjected to axial load and bending moment, as well the analytical formulation, it is shown in Figure 5 a generic rectangular section with known (or pre-defined) longitudinal reinforcement. Figure 5 also contains diagrams representing the section strains, the internal resultant forces, the stresses in the concrete and the internal resultant forces in the longitudinal reinforcement.

For the equilibrium of the horizontal forces, the applied axial force N_{Sd} must be equal to the sum of the resultant internal forces of concrete and reinforcement:

$$N_{Sd} = R_{cc} + \sum A_{si} \cdot \sigma_{si} - R_{ct} \tag{14}$$

where
R_{cc} is the resultant of the concrete compressive stresses;
R_{ct} is the resultant of concrete tensile stresses;
A_{si} is the area of the longitudinal reinforcement steel bar i (or layer i):
σ_{si} is the stress in the longitudinal reinforcement steel bar i (or layer i) (positive sign for compression).

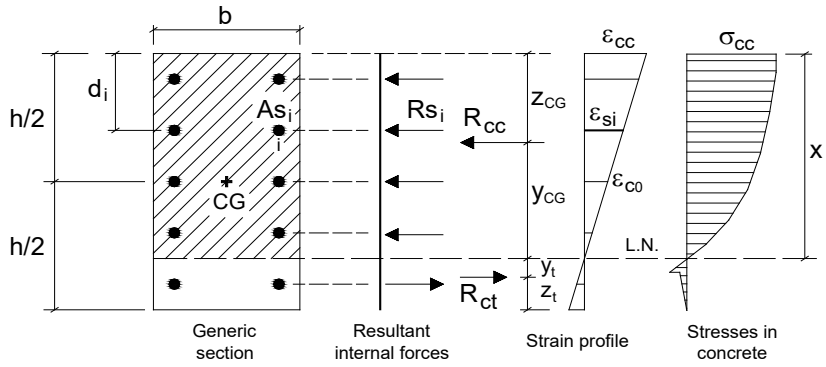

Figure 5. Generic rectangular section - strains, stresses in concrete and internal resultant forces

The moment resulting by the internal forces of the section in relation to the center of gravity of the concrete gross section can be calculated by Equation 15:

$$M = R_{cc} \cdot \left(\frac{h}{2} - z_{CG} \right) + \Sigma A_{si} \cdot \sigma_{si} \cdot \left(\frac{h}{2} - d_i \right) + R_{ct} \cdot \left(\frac{h}{2} - z_t \right) \tag{15}$$

where

h is the section height;

d_i is the distance between extreme compression fiber of the section and the steel bar i (or layer i) of the longitudinal reinforcement;

z_{CG} is the distance between extreme compression fiber of the section and resultant of the compressive stresses in the concrete R_{cc}. According to Figure 5, this distance is obtained by:

$$z_{CG} = x - y_{CG} \tag{16}$$

where:

x is the neutral axis depth;

y_{CG} is the distance from the neutral axis to the centroid of the compressive stress in concrete along the section height. This distance defines the point of application of the resultant R_{cc}. Likewise, the distances y_t and z_t define the position of the tensile resultant R_{ct}.

The formulation for sections subjected to axial load and bending moment follows the cases of strains presented in items 4.1.1 to 4.1.4. To verify the case in which the section is found, obtain the stresses in the longitudinal reinforcements, and generate the points of the moment-curvature curve, strain compatibility equations are used, according to Equation 17.

$$\frac{1}{r} = \frac{\varepsilon_{cc}}{x} = \frac{\varepsilon_{c0}}{x - h/2} = \frac{\varepsilon_{si}}{x - d_i} \text{ (positive sign for compression)} \tag{17}$$

where

$1/r$ is the section curvature;

ε_{cc} is the strain of the concrete extreme compression fiber;

ε_{c0} is the strain at the gross section centroid;

ε_{si} is the strain of the longitudinal reinforcement steel bar i (or layer i).

The constitutive models for concrete in compression and non-prestressed steel reinforcement according to NBR 6118 [1] are illustrated in Figure 6.

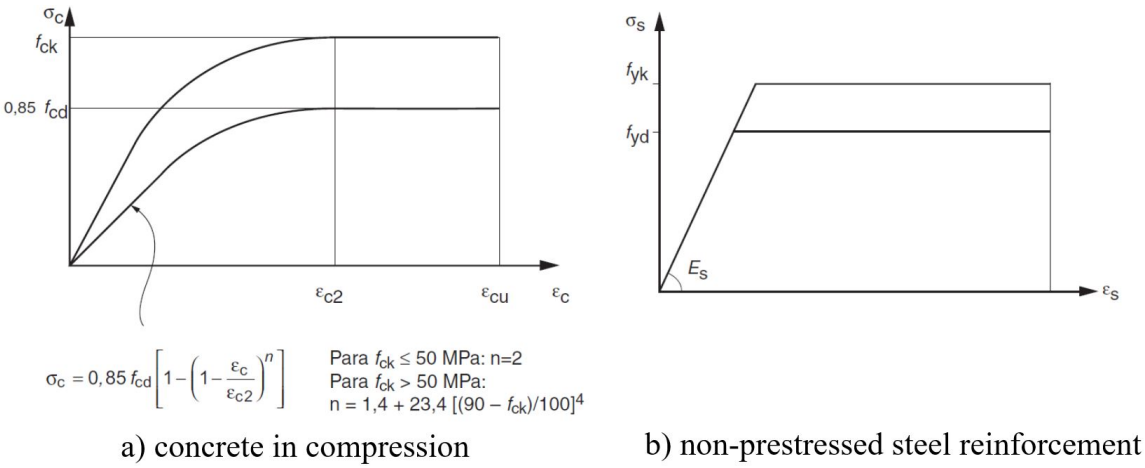

Figure 6. Idealized stress-strain curves for materials – NBR 6118 [1]

In Figure 6:

f_{ck} and f_{cd} are the concrete compressive strength (the characteristic and the design values, respectively);

ε_{c2} is the strain of beginning of plastification of the concrete (equal to 2 ‰ for concrete up to C50);

ε_{cu} is the ultimate strain of the concrete (assumed equal to 3,5 ‰ for concrete up to C50).

The curvature value is chosen and a value ε_{c0} is estimated (which can be done from the applied axial force at the first point of the curve) for the generation of a point of the moment-curvature diagram. An iterative process begins until the equilibrium of forces occurs in the section. The detailed solution algorithm is presented in item 4.1.6.

To deduce the analytical expressions for the compressive resultant in the concrete R_{cc} and its position in relation to the neutral axis y_{CG}, Equation 18 is used, which expresses the proportionality between the strain and the ordinate y, (Figure 7) - consequence of the assumption that plane sections remain plane.

$$\varepsilon_c = k \cdot y \tag{18}$$

where k is the constant that relates the concrete strain and the ordinate y. This constant represents the curvature of the section.

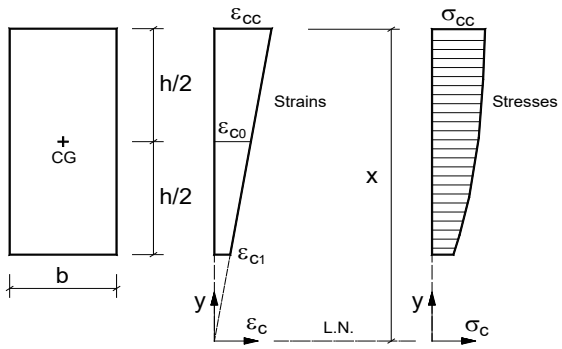

Figure 7: General scheme of strains and stresses in concrete along the section height

The analytical expressions for the compressive resultant in the concrete R_{cc} and its position in relation to the neutral axis y_{CG} for concretes C20 to C50 are presented in items 4.1.1 to 4.1.4. Depending on the strain of the extreme compression fiber of concrete ε_{cc} and the value of the neutral axis depth x, 4 possible cases are defined for sections subjected to axial load and bending moment, as shown in Figure 8.

In this paper, the values of strains in the concrete are expressed in units per thousand, due to the values assumed by ε_{c2} and by the exponent n of the parabolic function of the stress-strain curve for concretes up to C50. Thus, the values of y_{c2} (ordinate corresponding to the strain ε_{c2} according to Figure 8) are calculated by:

$$y_{c2} = \frac{\varepsilon_{c2}}{k} = \frac{2}{k} \quad (\varepsilon_{c2} \text{ in units per thousand}) \tag{19}$$

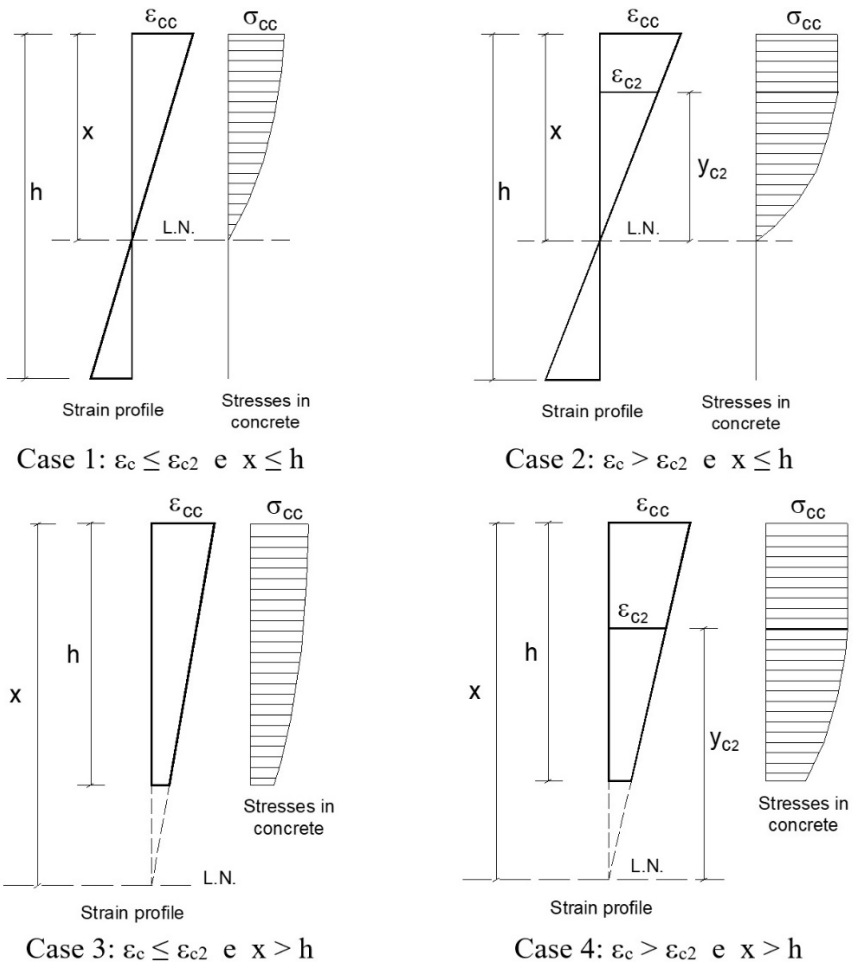

Figure 8. Possible cases - RC sections subjected to axial compressive load and bending moment

4.1.1 Case 1: $\varepsilon_{cc} \leq \varepsilon_{c2}$ e $x \leq h$

In this case, the neutral axis passes through the section and the concrete has not yet reached its maximum stress (strength). The resultant R_{cc} is calculated from the integration of the stresses over the compressed area of concrete:

$$R_{cc} = \int_0^x \sigma_c \cdot b \cdot dy = b \cdot \int_0^x \sigma_c \cdot dy \tag{20}$$

where
b is the section width (constant for rectangular section);
σ_c is the compressive stress of concrete as a function of the neutral axis depth x. In this case, the stress diagram takes on a parabolic format as shown in Figure 6.
The position of the resultant R_{cc} in the section is defined with the calculation of y_{CG}, expressed by:

$$y_{CG} = \frac{\int_0^x \sigma_c \cdot b \cdot y \cdot dy}{\int_0^x \sigma_c \cdot b \cdot dy} = \frac{b \cdot \int_0^x \sigma_c \cdot y \cdot dy}{R_{cc}} \tag{21}$$

Equation 22 can be deduced from substituting the analytical expression of the parabola that describes the compressive stress of the concrete in the integral of Equation 20:

$$R_{cc} = b \cdot \int_0^x 0,85 \cdot f_{cd} \cdot \left[1 - \left(1 - \frac{\varepsilon_c}{2} \right)^2 \right] \cdot dy \tag{22}$$

From Equation 18, it is possible to rewrite R_{cc} according to the ordinate y:

$$R_{cc} = 0,85 \cdot f_{cd} \cdot b \cdot \int_0^x \left[1 - \left(1 - \frac{k \cdot y}{2} \right)^2 \right] \cdot dy \tag{23}$$

Solving the integral expressed in Equation 23, results in:

$$R_{cc} = 0,85 \cdot f_{cd} \cdot b \cdot k \cdot \left(\frac{x^2}{2} + \frac{k \cdot x^3}{12} \right) \tag{24}$$

In the numerator of Equation 21, the analytical expression of the parabolic curve of the concrete compressive stress is used to calculate the integral:

$$y_{CG} = \frac{b \cdot \int_0^x 0,85 \cdot f_{cd} \cdot \left[1 - \left(1 - \frac{\varepsilon_c}{2} \right)^2 \right] \cdot y \cdot dy}{R_{cc}} \tag{25}$$

From Equation 18, it is possible to rewrite y_{CG} as a function of the ordinate y:

$$y_{CG} = \frac{0,85 \cdot f_{cd} \cdot b \cdot \int_0^x \left[1 - \left(1 - \frac{k \cdot y}{2} \right)^2 \right] \cdot y \cdot dy}{R_{cc}} \tag{26}$$

Solving the integral of the numerator of Equation 26 results in:

$$y_{CG} = \frac{16 \cdot x^3 - 3 \cdot k \cdot x^4}{24 \cdot x^2 - 4 \cdot k \cdot x^3} \tag{27}$$

4.1.2 Case 2: $\varepsilon_{cc} > \varepsilon_{c2}$ *e* $x \leq h$

The resultant R_{cc} and its position in the section represented by y_{CG} are calculated from the integration of the concrete compressive stresses over two regions: where the stresses assume parabolic distribution and in where the stresses assume a constant value equal to $0,85.f_{cd}$ (Figure 8).

$$R_{cc} = \int_{0}^{y_{c2}} \sigma_c \cdot b \cdot dy + \int_{y_{c2}}^{x} 0,85 \cdot f_{cd} \cdot b \cdot dy \tag{28}$$

$$y_{CG} = \frac{\int_0^{y_{c2}} \sigma_c \cdot b \cdot y \cdot dy + \int_{y_{c2}}^{x} 0,85 \cdot f_{cd} \cdot b \cdot y \cdot dy}{\int_0^{y_{c2}} \sigma_c \cdot b \cdot dy + \int_{y_{c2}}^{x} \sigma_c \cdot b \cdot dy} = \frac{b \cdot \int_0^{y_{c2}} \sigma_c \cdot y \cdot dy + 0,85 \cdot f_{cd} \cdot b \cdot \int_{y_{c2}}^{x} y \cdot dy}{R_{cc}} \tag{29}$$

Solving the integrals of Equations 28 and 29 provides the expressions for R_{cc} and y_{CG}:

$$R_{cc} = 0,85 \cdot f_{cd} \cdot b \cdot \left(k \cdot \frac{{y_{c2}}^2}{2} - k^2 \cdot \frac{{y_{c2}}^3}{12} + x - y_{c2} \right) \tag{30}$$

In Equation 29, substituting the parabolic function that describes the compressive stress in concrete σ_c and using Equation 18 that relates ε_c and y result in:

$$y_{CG} = \frac{0,85 \cdot f_{cd} \cdot b}{R_{cc}} \left(\frac{k \cdot {y_{c2}}^3}{3} - \frac{k^2 \cdot {y_{c2}}^4}{16} + \frac{k \cdot x^2}{2} - \frac{k \cdot {y_{c2}}^2}{2} \right) \tag{31}$$

4.1.3 Case 3: $\varepsilon_{cc} \leq \varepsilon_{c2}$ **e** $x > h$

In this case, the section is completely compressed, and the concrete has not yet reached its maximum stress (strength). The integrals used for the calculation of R_{cc} and y_{CG} must be calculated within the range of ordinates y that cover the section, according to Equations 32 and 33.

$$R_{cc} = \int_{x-h}^{x} \sigma_c \cdot b \cdot dy = b \cdot \int_{x-h}^{x} \sigma_c \cdot dy \tag{32}$$

$$y_{CG} = \frac{\int_{x-h}^{x} \sigma_c \cdot b \cdot y \cdot dy}{\int_{x-h}^{x} \sigma_c \cdot b \cdot dy} = \frac{b \cdot \int_{x-h}^{x} \sigma_c \cdot y \cdot dy}{R_{cc}} \tag{33}$$

Solving the integrals of Equations 32 and 33 provides the expressions for R_{cc} and y_{CG}:

$$R_{cc} = 0,85 \cdot f_{cd} \cdot b \cdot k \cdot \left[\frac{x^2}{2} - \frac{(x-h)^2}{2} - \frac{k \cdot x^3}{12} + \frac{k \cdot (x-h)^3}{12} \right] \tag{34}$$

$$y_{CG} = \frac{0,85 \cdot f_{cd} \cdot b \cdot k \cdot \left[\frac{x^3}{3} - \frac{(x-h)^3}{3} - \frac{k \cdot x^4}{16} + \frac{k \cdot (x-h)^4}{16} \right]}{R_{cc}} \tag{35}$$

4.1.4 Case 4: $\varepsilon_{cc} > \varepsilon_{c2}$ e $x > h$

In the same way as case 2, R_{cc} and y_{CG} are calculated from the integration of the concrete compressive stresses over two regions: for the parabolic segment and for the constant stress segment. The complete integration interval comprises the entire height of the section.

$$R_{cc} = \int_{x-h}^{y_{c2}} \sigma_c \cdot b \cdot dy + \int_{y_{c2}}^{x} b \cdot \sigma_c \cdot dy = b \cdot \left(\int_{x-h}^{y_{c2}} \sigma_c \cdot dy + 0,85 \cdot f_{cd} \cdot \int_{y_{c2}}^{x} \sigma_c \cdot dy \right) \tag{36}$$

$$y_{CG} = \frac{\int_{x-h}^{y_{c2}} \sigma_c \cdot b \cdot y \cdot dy + \int_{y_{c2}}^{x} b \cdot \sigma_c \cdot y \cdot dy}{\int_{x-h}^{y_{c2}} \sigma_c \cdot b \cdot dy + \int_{y_{c2}}^{x} b \cdot \sigma_c \cdot dy} = \frac{b \cdot \left(\int_{x-h}^{y_{c2}} \sigma_c \cdot y \cdot dy + \int_{y_{c2}}^{x} \sigma_c \cdot y \cdot dy \right)}{R_{cc}} \tag{37}$$

Solving the integrals of Equations 36 and 37 provides the expressions for R_{cc} and y_{CG}:

$$R_{cc} = 0,85 \cdot f_{cd} \cdot b \cdot \left[\frac{k \cdot {y_{c2}}^2}{2} - \frac{k \cdot (x-h)^2}{2} - \frac{k^2 \cdot {y_{c2}}^3}{12} + \frac{k^2 \cdot (x-h)^3}{12} + x - y_{c2} \right] \tag{38}$$

$$y_{CG} = \frac{0,85 \cdot f_{cd} \cdot b}{R_{cc}} \left[\frac{k \cdot {y_{c2}}^3}{3} - \frac{k \cdot (x-h)^3}{3} - \frac{k^2 \cdot {y_{c2}}^4}{16} + \frac{k^2 \cdot (x-h)^4}{16} + \frac{x^2}{2} - \frac{{y_{c2}}^2}{2} \right] \tag{39}$$

4.1.5 Tension Stiffening

For considering the contribution of tensioned concrete between cracks (tension stiffening), Torres et al. [11] model was used, which assumes a stress-strain curve for concrete in tension as shown in Figure 9.

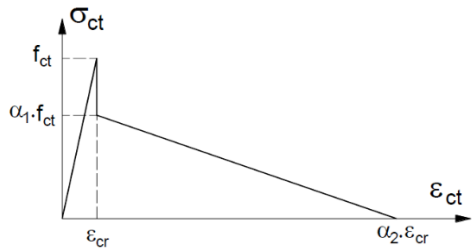

Figure 9. Equivalent stress-strain curve for concrete in tension (tension stiffening) – Torres et al. [11]

In Figure 9:

f_{ct} is the tensile concrete strength (peak value);

ε_{cr} is the strain corresponding to the maximum tensile stress (peak value);

α_1 and α_2 are the coefficients which define the tension stiffening model and are obtained with Equations 40 and 41:

$$\alpha_1 = 0,4 \cdot \left(1 - \frac{N}{A \cdot f_{ct}} \right) \geq 0 \tag{40}$$

$$\alpha_2 = 20,3 - 15,1 \cdot \frac{d}{h} + \frac{1,31}{\alpha_e \cdot \rho} - \frac{1,06}{\alpha_e \cdot \rho} \cdot \frac{d}{h} \tag{41}$$

where
N is the axial compressive force (positive sign for compression);
A is the cross-section area;
d is the cross-section effective depth;
h is the cross section total height;
α_e is the ratio between the modulus of elasticity of steel to the concrete modulus of elasticity;
ρ is the tensile reinforcement ratio (related to the section effective depth).

The values α_1 and α_2 are calculated in case of tensile stresses in the section. The value of the tensile resultant in concrete R_{ct} and its position (with the distances y_t and z_t, as shown in Figure 5) are calculated using the equations of equilibrium and compatibility of the section.

4.1.6 Algorithm for generating the points of the moment-curvature diagrams

In a simplified way, the solution algorithm used in this paper for the generation of each point of the moment-curvature diagram is presented:
(1) Set the curvature value $1/r$
(2) Estimate the initial value $\varepsilon_{c0} = \dfrac{N_{Sd}}{E_{ci} \cdot (bh)}$
(3) Iterative Process: While ErrorN >Tolerance

$$\varepsilon_{cc} = \varepsilon_{c0} + 1/r \cdot \left(\frac{h}{2}\right)$$

$$x = \frac{\varepsilon_{cc}}{1/r}$$

$$k = \frac{\varepsilon_{cc}}{x}$$

(4) Identify the case applicable to members under bending and axial loads from ε_{cc} and x
(5) Calculate R_{cc}, y_{CG}, z_{CG}
(6) Calculate R_{ct}, y_t, z_t
(7) Calculate the strains (Equation 17) and the stresses in the reinforcements
(8) Calculate $M = R_{cc} \cdot \left(\frac{h}{2} - Z_{CG}\right) + \sum A_{si} \cdot \sigma_{si} \cdot \left(\frac{h}{2} - d_i\right) + R_{ct} \cdot \left(\frac{h}{2} - Z_t\right)$
(9) Calculate $N = R_{cc} + \sum A_{si} \cdot \sigma_{si} - R_{ct}$
(10) Calculate $\Delta\varepsilon_{c0} = \dfrac{N_{Sd} - N}{E_{ci} \cdot (bh)}$
(11) Recalculate $\varepsilon_{c0} = \varepsilon_{c0} + \Delta\varepsilon_{c0}$
(12) Calculate $ErrorN = \dfrac{|N_{Sd} - N|}{b \cdot h \cdot f_{cd}}$
(13) Return to step (3) and check the end of the iterative process

In the presented algorithm, ErrorN is associated with the relative error in terms of axial force. Tolerance must be defined: values around 0.001 (0.1%) are sufficient to achieve good accuracy.

4.2 Equivalent Branson stiffness (beams only)

A simpler alternative than that presented in item 4.1 in beams is the use of the expression suggested by Branson [12] to calculate the equivalent flexural stiffness in Stage II (cracked). Thus, the moment-curvature curve is defined by the

cracking moment, by the ultimate moment (strength) - both calculated by usual design of reinforced concrete sections - and by the segment obtained by relations indicated in Equations 42 and 43 corresponding to Stage II:

$$\frac{1}{r} = \frac{M}{(EI)_{eq}} \tag{42}$$

$$(EI)_{eq} = E_c \cdot \left\{ \left(\frac{M_r}{M} \right)^3 .I_I + \left[1 - \left(\frac{M_r}{M} \right)^3 \right] .I_{II} \right\} \tag{43}$$

where

E_c is the concrete modulus of elasticity;

M_r it is the cracking moment;

M it is the section applied moment;

I_I is the uncracked section second moment of area (inertia, Stage I);

I_{II} it is the cracked section second moment of area (inertia, Stage II).

The moment-curvature diagrams of the reinforced concrete beam for one of the connections analyzed by numerical simulations of item 5 (LVP1) is shown in Figure 10 for the purpose of comparison between the differences found when using the equilibrium equations of the section (item 4.1) and when using Branson expression in the Stage II.

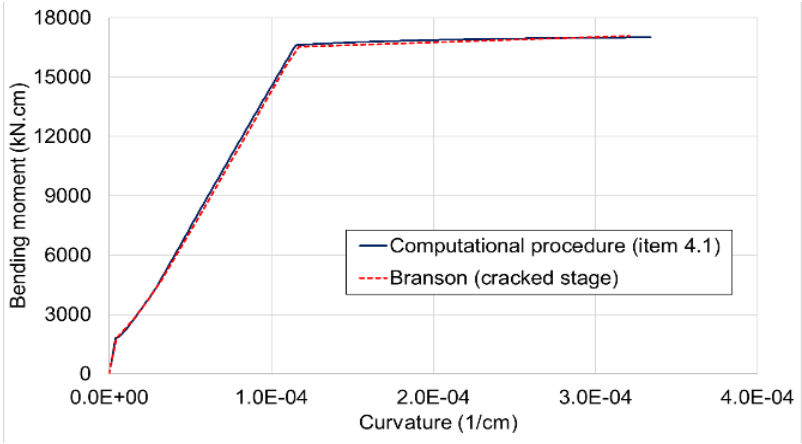

Figure 10. Moment-curvature curves generated using computational procedure (item 4.1) and using Branson´s expression (cracked stage) for LVP1: Alva [13]

5 NUMERICAL SIMULATIONS

In this item, numerical simulations of beam-column connections of reinforced concrete frames are presented for the comparison between theoretical and experimental results. To obtain the theoretical results, the analytical model proposed by Alva and El Debs [8] was applied to account for the deformability under bending moment (item 3). Moment-curvature relationships (as per item 4) were used in the consideration of the material nonlinearity.

Figure 11 illustrates the geometry of the beam-column connections analyzed by the numerical simulations, as well as the loading scheme applied and the longitudinal reinforcement of beams and columns of these connections.

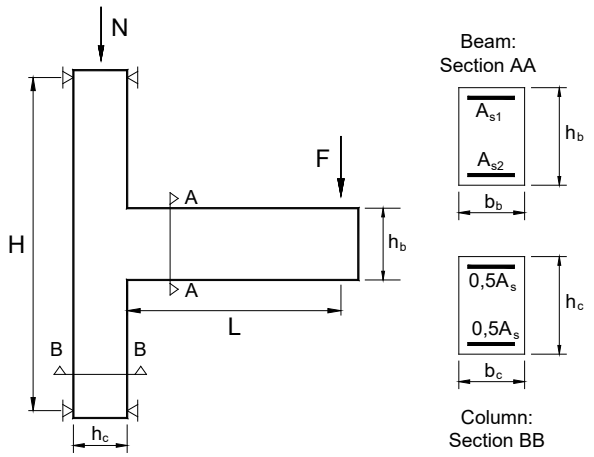

Figure 11. Detail of the beam-column connections of the numerical simulations

The mechanical characteristics are summarized in Table 1 (concrete and longitudinal reinforcements). The dimensions of the connections and the area of longitudinal reinforcements of beams and columns are shown in Table 2. Table 3 contains the constants values of the model presented in Alva and El Debs [8] for the connections analyzed by the numerical simulations. It should be noted that all parameters of the analytical model were calculated based on the mechanical properties of the materials (characterization tests).

Table 1. Mechanical properties of concrete and longitudinal steel reinforcement of the beam-column connections

Connection		f_c (MPa)	f_{ct} (MPa)	E_c (GPa)	f_y (MPa)	E_s (GPa)
Alva [13]	LVP1	44,18	3,30	33,60	630	182
	LVP2	23,89	1,95	28,32	594	213
	LVP3	24,62	2,08	28,47	594	213
	LVP4	25,91	2,20	28,74	594	213
Lee et al. [14]	Specimen 2	28,94	2,89	25,91	335	200
	Specimen 5	24,80	2,48	23,70	351	200

f_c – concrete compressive strength f_{ct} – concrete tensile strength. E_c – modulus of elasticity of concrete. f_y – yield stress of steel reinforcement. E_s – modulus of elasticity of steel reinforcement

Table 2. Dimensions and area of the longitudinal reinforcement of the beam-column connections

Connections	L (cm)	H (cm)	h_b (cm)	b_b (cm)	h_c (cm)	b_c (cm)	A_{s1} (cm^2)	A_{s2} (cm^2)	A_s (cm^2)
Alva [13] LVP1-LVP4	155,0	250,0	40,0	20,0	30,0	20,0	8,04	8,04	20,10
Lee et al. [14] Specimen 2	118,1	152,4	25,4	20,3	27,9	20,3	5,70	4,00	11,35
Lee et al. [14] Specimen 5	104,8	152,4	25,4	20,3	27,9	20,3	5,70	4,00	11,35

Table 3. Constants of Alva and El Debs [8] analytical model

Connections		M_y (kN.cm)	ϕ (mm)	L_p (cm)	s_R (cm)	C_1 $(kN.cm)^{-2}$	C_2 (cm)
Alva [13]	LVP1	16577	16	30	12,9	9,526E-12	21,45
	LVP2	15645	16	30	12,9	7,861E-12	21,45
	LVP3	15369	16	30	12,9	1,132E-11	21,45
	LVP4	15380	16	30	12,9	1,114E-11	21,45
Lee et al. [14]	Specimen 2	3298	19	20,3	17,2	1,609E-10	18,76
	Specimen 5	3458	19	20,3	17,2	1,774E-10	18,73

5.1 Beam-column connections: Alva [13]

Alva [13] performed tests on exterior beam-column connections subjected to alternating cyclic loads. The first stage of loading was the same to all connections: application of cyclic loads with amplitude increments of 10 kN up to the value of 60 kN. This loading in the first cycle generated a maximum bending moment corresponding to 60% of the yielding moment. Higher loads were applied at the end of the beam in the second stage of loading until the failure of the connection, as shown in Figure 12.

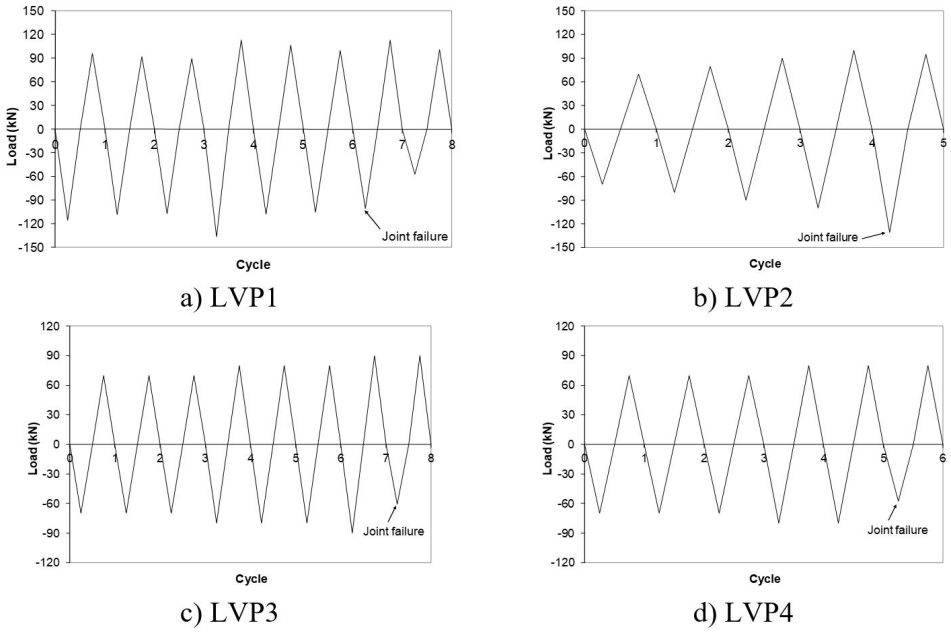

Figure 12. Loading history at the last stage of loading - Alva [13]

In all connections, the failure occurred by crushing the diagonal strut due to beam-column joint shear forces. In the connections LVP1 and LVP2, the connection failure occurred with yielding of the beam flexural reinforcement. In the connections LVP3 and LVP4, the failure of the connection occurred without the yielding of the beam flexural reinforcement. Further information about the experimental investigation is found in Alva [13] and Alva and El Debs [8].

To obtain the relative rotations between beam and column, horizontal displacement transducers were used, as shown in Figure 13.

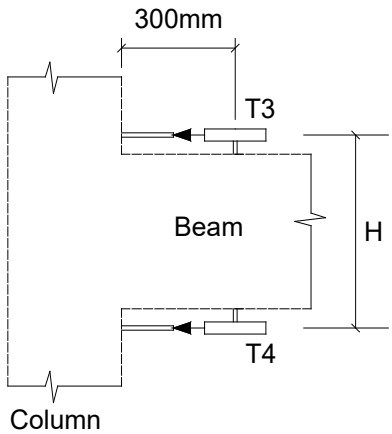

Figure 13. Displacement transducers used to evaluate relative rotations - Alva [13]

In this case the relative rotation is calculated by:

$$\theta = \frac{\delta_3 - \delta_4}{H} \tag{44}$$

where δ_3 and δ_4 are the displacements measured by the transducers T3 and T4 and H is the distance between the transducers.

According to Figure 13, the length L_p to be used in Alva and El Debs [8] model is equal to 300 mm (see transducers position in relation to the column face).

The moment-rotation curves of the connections tested by Alva [13] are shown in Figures 14 to 17 for the two stages of loading mentioned.

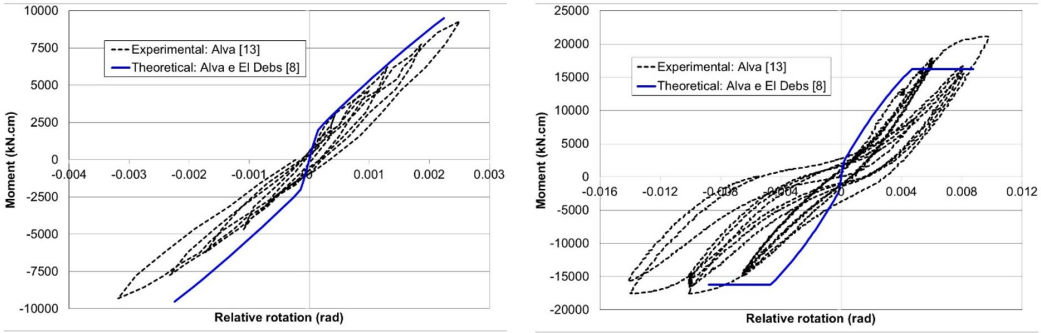

a) First stage of loading b) Last stage of loading

Figure 14. Experimental and theoretical moment-rotation curves for LVP1 - Alva [13]

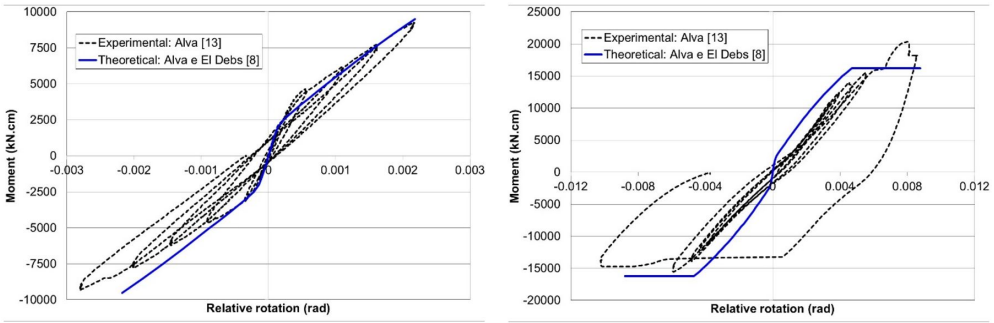

a) First stage of loading b) Last stage of loading

Figure 15. Experimental and theoretical moment-rotation curves for LVP2 - Alva [13]

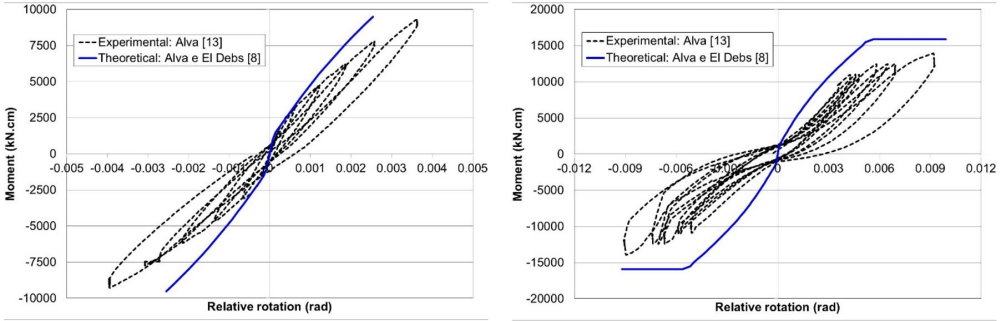

a) First stage of loading b) Last stage of loading

Figure 16. Experimental and theoretical moment-rotation curves for LVP3 - Alva [13]

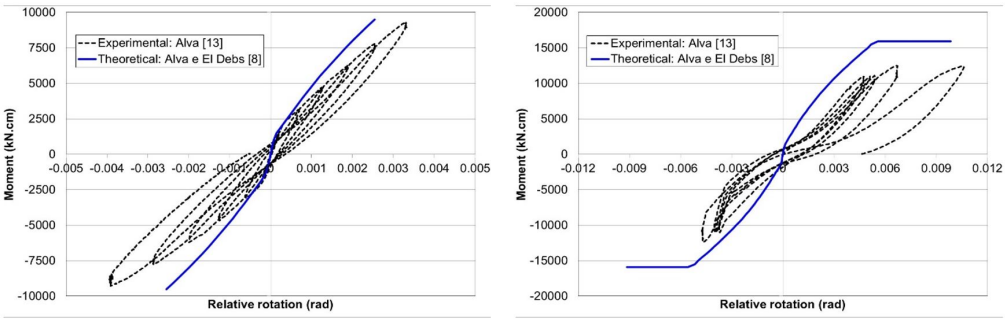

a) First stage of loading b) Last stage of loading

Figure 17. Experimental and theoretical moment-rotation curves for LVP4 - Alva [13]

In a general way, it can be concluded that Alva and El Debs [8] analytical model simulates satisfactorily the bending deformability of the connections. For the second loading stage of the connections LVP3 and LVP4, the results provided by the analytical model were less satisfactory, since the shear joint failure did not allow the connection to reach the yielding moment of the beams.

5.2 Beam-column connections: Lee et al. [14]

Lee et al. [14] presented experimental results of beam-column connections subjected to seismic loads. Specimen 2 and Specimen 5 were chosen for comparison with the theoretical results. Figure 18 illustrates the structural model used to obtain the theoretical force-displacement curves using the finite element software ANSYS. The moment-rotation behavior of the beam-column connections was simulated by nonlinear springs, using the COMBIN39 element. The joint region was simulated with rigid offsets. Beams and columns were discretized and represented by frame elements, using the finite element BEAM188, which allows the consideration of material nonlinearity by moment-curvature relationships. The points of the moment-curvature curves were obtained by the formulation presented in item 4. The iterative incremental Newton-Raphson method was used for the numerical solution of the nonlinear problem, with convergence criteria based on the residual forces and moments.

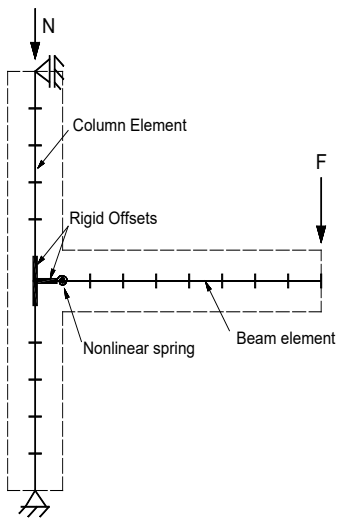

Figure 18. Structural model for obtaining the theoretical curves - Lee et al. [14]

Figure 19 contains the theoretical force-displacement curves (fully rigid and deformable connections) and the experimental curve for the first loading cycle. It can be seen from the referred curves that the consideration of the bending deformability led to significantly better results than those obtained by the hypothesis of a fully rigid connection.

There are no experimental results from moment-rotation curves in Lee et al. [14]. Thus, the experimental relative rotations between beam and column were obtained indirectly from the experimental displacements, according to Equation 45:

$$\theta = \frac{\delta_{exp} - \delta_{teor}}{L} \tag{45}$$

where

δ_{exp} is the experimental displacement at the beam end at the loading point;

δ_{teor} is the theoretical displacement at the beam end obtained by the hypothesis of fully rigid connection;

L is the distance from the load application point at the beam end to the face of the column.

Figure 20 contains the experimental moment-rotation curves (obtained indirectly by Equation 45) and the curves obtained using Alva and El Debs [8] analytical model. The comparison of results reveals that the analytical model simulates in a very satisfactory way the bending deformability of the beam-column connections.

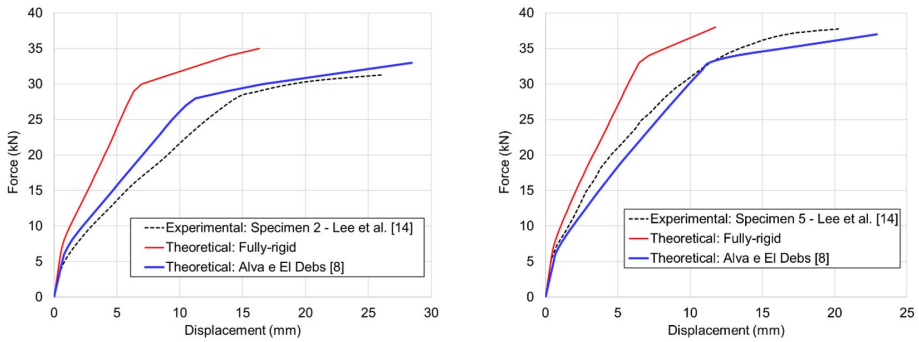

a) Specimen 2 b) Specimen 5

Figure 19. Experimental and theoretical force-displacement curves - Lee et al. [14]

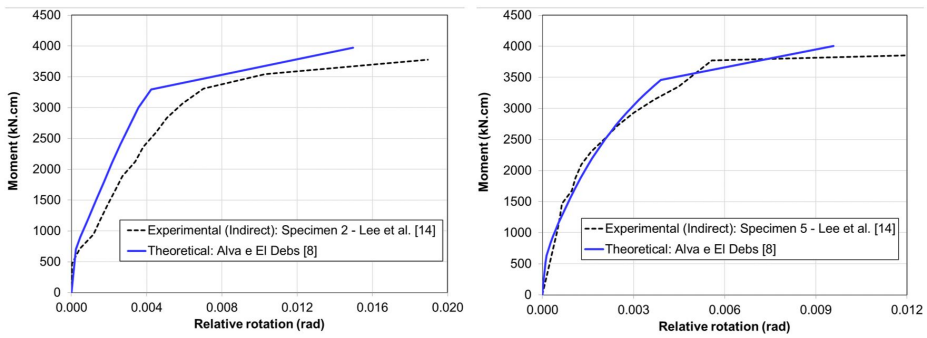

a) Specimen 2 b) Specimen 5

Figure 20. Experimental and theoretical moment-rotation curves - Lee et al. [14]

6 FINAL CONSIDERATIONS AND CONCLUSIONS

This paper dealt with the question of the deformability of reinforced concrete monolithic beam-column connections in the nonlinear analysis of framed reinforced concrete structures. To consider the deformability under bending moment, Alva and El Debs [8] analytical model was used. To consider the material nonlinearity of structural elements, moment-curvature relationships were used. The entire formulation of the constitutive models was deduced and presented, to allow the implementation of these models in computational procedures.

The numerical simulations carried out in this paper prove that taking into account the bending deformability of the connections leads to significantly better results than the hypothesis of fully rigid connections, even in the case of monolithic connections. In addition, Alva and El Debs [8] model proved to be suitable for use in structural models that employ moment-curvature relationships in nonlinear analysis of reinforced concrete frames.

ACKNOWLEDGEMENTS

To CNPq for the financial support to the first author (Process: 308720/2018-0). To CAPES for the financial support to the second author (Process: 1769743).

REFERENCES

[1] Associação Brasileira de Normas Técnicas, *Projeto de Estruturas de Concreto – Procedimento*, NBR 6118, 2014.

[2] P. Paultre, D. Castele, S. Rattray, and D. Mitchell, "Seismic response of reinforced concrete frame subassemblages – a Canadian code perspective," *Can. J. Civ. Eng.*, vol. 16, no. 5, pp. 627–649, 1989, http://dx.doi.org/10.1139/l89-097.

[3] H. Sezen and J. Moehle, "Bond-slip behavior of reinforced concrete members," in *Proc. Fib Symp. (CEB-FIP) – Concr. Struct. Seismic Reg.*, 2003, pp. 1-10.

[4] H. Sezen and E. Setzler, "Reinforcement slip in reinforced concrete columns," *ACI Struct. J.*, vol. 105, no. 3, pp. 280–289, 2008.

[5] H. Kwak and S. Kim, "Simplified monotonic moment-curvature relation considering fixed-end rotation and axial force effect," *Eng. Struct.*, vol. 32, no. 1, pp. 69–79, 2010, http://dx.doi.org/10.1016/j.engstruct.2009.08.017.

[6] M. Ferreira, M. El Debs, and K. Elliott, "Determinação analítica da relação momento-rotação em ligações viga-pilar de estruturas pré-moldadas de concreto," in *An. Simp. EPUSP Estrut. Concr.*, 2003, pp. 1-20.

[7] G. Alva, M. Ferreira, and A. El Debs, "Partially restrained beam-column connections in reinforced concrete structures," *Ibracon Struct. Mater. J.*, vol. 2, no. 4, pp. 356–379, 2009., http://dx.doi.org/10.1590/S1983-41952009000400004.

[8] G. Alva and A. El Debs, "Moment–rotation relationship of RC beam-column connections – experimental tests and analytical model," *Eng. Struct.*, vol. 56, pp. 1427–1438, 2013, http://dx.doi.org/10.1016/j.engstruct.2013.07.016.

[9] European Committee for Standardization, *Design of Concrete Structures – Part 1: General Rules and Rules for Building*, Eurocode 2, 2004.

[10] G. Alva, "Formulação analítica para a determinação de diagramas momento-curvatura em seções de concreto armado retangulares submetidas à flexão normal composta," in *An. 59° Congr. Bras. Concr.*, 2017, pp. 1-16.

[11] L. I. Torres, F. López-Almansa, and L. Bozzo, "Tension-stiffening model for cracked flexural concrete members," *J. Struct. Eng.*, vol. 130, no. 8, pp. 1242–1251, 2004, http://dx.doi.org/10.1061/(ASCE)0733-9445(2004)130:8(1242).

[12] D. Branson, *Instantaneous and Time-dependent Deflections of Simple and Continuous Reinforced Concrete Beams* (HPR Publication 7 part 1). Alabama: Alabama High. Depart., U. S. Bur. Publ. Roads, 1965, pp. 1-78.

[13] G. Alva, "Estudo teórico-experimental do comportamento de nós de pórtico de concreto armado submetidos a ações cíclicas," Ph.D. dissertation, Esc. Eng. São Carlos, Univ. São Paulo, São Carlos, 2004. [Online]. Available: http://www.teses.usp.br

[14] L. Lee, J. Wight, and R. Hanson, "RC beam-column joints under large load reversals," *J. Struct. Div.*, vol. 103, no. 12, pp. 2337–2350, 1977.

Author contributions: Gerson Alva (G.A.): conceptualization, data curation, formal analysis, investigation, methodology, validation, writing. Alexandre Tsutake (A.T.): investigation, methodology, validation, writing.

Editors: Osvaldo Luís Manzoli, José Luiz Antunes de Oliveira e Sousa, Guilherme Aris Parsekian.